JOURNAL OF AGRICULTURAL AND FOOD CHEMISTRY

Article

pubs.acs.org/JAFC

Fabrication and Characterization of Novel Antimicrobial Films Derived from Thymol-Loaded Zein−Sodium Caseinate (SC) Nanoparticles

Kang-Kang Li,[†] Shou-Wei Yin,*[,†,‡,#] Xiao-Quan Yang,*[,†] Chuan-He Tang,[†] and Zi-Hao Wei[†]

[†]Research and Development Center of Food Proteins, Department of Food Science and Technology, South China University of Technology, Guangzhou 410640, People's Republic of China

[‡]State Key Laboratory of Pulp and Paper Engineering, South China University of Technology, Guangzhou 510640, People's Republic of China

[#]Guangdong Province Key Laboratory for Green Processing of Natural Products and Product Safety, South China University of Technology, Guangzhou 510640, People's Republic of China

ABSTRACT: The objective of this research was to fabricate novel antimicrobial films based on zein colloidal nanoparticles coated with sodium caseinate (SC), an emulsifier/stabilizer. Thymol-loaded zein−SC nanoparticles were prepared using an antisolvent technique, with the average particle size and zeta potential about 200 ± 20 nm and −40 mV, respectively. Zein−SC nanoparticle-based films exhibited higher mechanical resistance and water barrier capacity than the SC films and concomitant good extensibility as compared with zein films. Thymol loadings endowed zein−SC nanoparticle-based films with antimicrobial activity against *Escherichia coli* and *Salmonella* as well as DPPH radical scavenging activity. Water vapor permeability, microstructure, mechanical, and controlled release properties of the films were evaluated. The possible relationship between some selected physical properties and microstructure were also discussed. Atomic force microscopy (AFM) analysis indicated that thymol loadings resulted in the emergence phenomena of the nanoparticles to form large particles or packed structure, consisting of clusters of nanoparticles, within the film matrix, in a thymol loading dependent manner. The appearance of large particles or an agglomerate of particles may weaken the compactness of protein network of films and thus impair the water barrier capacity, mechanical resistance, and extensibility of the films. The release kinetics of thymol from nanoparticle-based films can be described as a two-step biphasic process, that is, an initial burst effect followed by subsequent slower release, and zein−SC nanoparticles within the films matrices gave them the ability to sustain the release of thymol. In addition, a schematic illustration of the formation pathway of zein−SC nanoparticle-based films with or without thymol was proposed to illuminate the possible relationship between some selected physical properties and the microstructure of the films.

KEYWORDS: *antimicrobial films, zein−SC nanoparticles, microstructure, thymol, sustained release*

INTRODUCTION

There is an increased demand for easily prepared, minimally processed fresh produce without any foodborne microbial contamination.[1,2] This has intensified the research on antimicrobial packaging technologies.[3] Food-packaging films allow a controlled release of the additives into the food over a prolonged time (including storage and distribution operations) and limit possible undesirable flavors caused by the direct addition of these additives into food.[2,4] Biopolymer-based films show a promising potential as a partial substitute for petroleum-based plastic package films to reduce environmental impact.[5] Among the biopolymer-based films, protein-based films are one of the most attractive due to their nutritional value as well as impressive gas barrier properties.[6] Zein, a proline-rich protein obtained from corn, has been studied as a potential biomaterial for delivery systems.[7,8] The water-insoluble characteristic of zein makes it a good candidate for the development of natural biopolymeric colloidal particles or films, which can be used for controlled delivery of drugs or other functional molecules such as antimicrobials.[9,10] However, zein-alone films were usually highly brittle and showed very little elongation,[10,11] which limited their usage in food packaging.

Due to the safety concern in the active food-packaging sector, formulations based on natural compounds are more desirable. Natural extracts such as essential oils or their main components, which are categorized as Generally Recognized as Safe (GRAS) by the U.S. Food and Drug Administration (FDA), could be considered potential alternatives to synthetic additives.[12,13] Thymol, the most abundant component of thyme (*Thymus vulgaris*), is formed via *p*-cymene from *γ*-terpinene.[14] Thymol possesses the GRAS status as defined by FDA. Its antimicrobial properties were investigated by in vitro and in vivo assay, demonstrating it is effective against natural spoilage bacteria and against foodborne pathogens, for example, *Salmonella typhimurium*, *Escherichia coli*, and *Listeria monocytogenes*.[15−18] The antibacterial activity of thymol may result, at least in part, from the disruption of a lipid layer of the cytoplasmic membrane of cells, which results in disruption of its continuity.[19]

Received: June 26, 2012
Revised: October 31, 2012
Accepted: November 5, 2012
Published: November 5, 2012

dx.doi.org/10.1021/jf302752v | *J. Agric. Food Chem.* 2012, 60, 11592−11600

Controlled release systems need to be fabricated for thymol to minimize the impact on the organoleptic properties of foods. The controlled release systems received a large amount of attention for their ability to carry the antimicrobial agent from the polymeric matrix to the food surface.[20] Recently, thymol was incorporated in zein films at thymol-to-zein ratios of 5−35%. The films with thymol-to-zein ratios of 20−35% were effective against selected spoilage foodborne microorganisms including *Bacillus cereus*, *Candida lusitaniae*, and *Pseudomonas* spp.[21] All thymol-loaded zein films show microvoids, and the size of the microvoids increases as the thymol concentration increases,[21] indicating that thymol loading may impair the physical properties of zein films. Mastromatteo et al.[22] investigated the release profiles of thymol-loaded mono- and multilayer zein films and indicated that the thymol release rate decreased with the increase of the film thickness. The addition of a natural filler, spelt bran, resulted in a significant increase of thymol release rate with the increase of fibril amounts.[22] This phenomenon may be due to a poor adhesion between fibers and the zein matrix, with subsequent increase in the porosity of the zein matrix.

Although some information on thymol-loaded zein films is available in the literature,[21,22] information about the films prepared from thymol-loaded nanoparticles is scarce. Sodium caseinate (SC) has been reported to act as an emulsifier/stabilizer due to the combination of electrostatic and steric stabilization.[23] Colloidal particles with well-defined size ranges (120−150 nm) and negative surface potential (−29 to −47 mV) were obtained based on zein and SC using a simple antisolvent method.[24] These nanoscale particles have already been explored to design colloidal delivery systems for curcumin, indicating that the particles have good colloidal stability at a broad range of physiologically relevant pH and in simulated gastrointestinal conditions.[25] However, the properties of the films derived from the thymol-loaded zein−SC nanoparticles were completely unknown.

Thus, the objectives of this work are to develop novel edible thymol-loaded films derived from zein−SC nanoparticles. Antibacterial properties, antioxidant capacity, and the release dynamics of thymol of the films were evaluated. Water vapor barrier, microstructure, and mechanical properties of the films were investigated. In addition, a schematic illustration of the formation pathway of zein−SC nanoparticle-based films with or without thymol was proposed to explore the possible relationship between some selected physical properties and the microstructure of the films.

MATERIALS AND METHODS

Materials. Thymol (95% purity) and zein were purchased from Sigma Chemical Co. (St. Louis, MO, USA). 1,1-Diphenyl-2-picrylhydrazyl radical 2,2-diphenyl-1-(2,4,6-trinitrophenyl)hydrazyl (DPPH) was also purchased from Sigma Chemical Co. Sodium caseinate (food grade) was purchased from Murray Goulburn Co-operative Co. Limited, Australia. All other chemicals used were of analytical grade.

Particle Synthesis. Zein particles were prepared using a modified method based on antisolvent procedure. Precisely, zein (5 g) was dissolved in 100 mL of ethanol/water binary solvent (80:20 v/v) to form a stock solution, and thymol was added to zein solution at thymol-to-zein ratios of 0, 0.1, 0.2, 0.3, and 0.4 g g^{-1}, respectively. Then, 250 mL of Milli-Q water with 2% w/v SC was immediately poured into the zein solution at a zein/SC ratio of 1:1, under continuous stirring (1000 rpm) using a magnetic stirrer. The final dispersions, at pH 6.6−6.8, were used to prepare films or stored at 4 °C until used for evaluation of particle size, shape, and zeta potential.

Preparation of Zein−SC Nanoparticle-Based Films. After 0.6 g of glycerol had been mixed in, 70 mL of the above solution was cast onto rimmed, leveled glass plates wrapped with polyethylene films (Clorox China Co. Ltd., Guangzhou, China).The film thickness was controlled by casting the same solids (2.6 g) on each plate (18 × 20 cm). The castings were air-dried in a thermostatic and humidistatic chamber [25 ± 1 °C, 50 ± 5% relative humidity (RH)] for 48 h, and then the films were peeled off the plates.

Preparation of SC Films. Sodium caseinate aqueous solutions with protein concentrations of 5.0% (w/v) were prepared by dispersing SC powder in deionized water followed by continuous stirring for 1 h at room temperature. Appropriate amounts of glycerol were added to achieve a glycerol-to-protein ratio of 0.3 g g^{-1}. Following degassing under vacuum, the film-forming dispersion (FFD) was cast onto rimmed, leveled glass plates coated with polyethylene films (Clorox China Co. Ltd.). The film thickness was controlled by casting the same solids (2.8 g) on each plate (18 × 20 cm). The castings were air-dried in a thermostatic and humidistatic chamber (25 ± 1 °C, 50 ± 5% RH) for 48 h, and then the films were peeled off the plates.

Moisture Content (MC). The MC of films was determined by oven-drying at 105 ± 2 °C for 24 h and expressed as the percentage of initial film weight lost during drying.

Analysis of Particle Size and Surface Potential. The particle size and zeta potential of dispersions were measured by dynamic light scattering (DLS) using a Zetasizer Nano ZS (Malvern Instruments Ltd., UK) after appropriate dilutions. All measurements were carried out at 25 °C, and the results reported are the average of three readings.

Atomic Force Microscopy (AFM) Images. Surface topography of films was measured using AFM with a Multimode SPM and Nanoscope Ia controller (Veeco Instruments, Plainview, NY, USA). The films were cut to 2.5 × 2.5 mm and fixed on the sample stage with double-sided tape. The microscope was operated in the tap mode, wherein changes in the contact amplitude of the cantilever tip on the surface of the film provide feedback signals for measuring variations in surface topography. All AFM images were acquired from the air side of the films. The surface roughness of the films was calculated on the basis of the root-mean-square (RMS) deviation from the average height of peaks after subtracting the background using Nanoscript (Veeco Instruments) software according to the standard ASME B46.1.14.

Tensile Strength (TS) and Elongation at Break (EAB). TS and EAB were measured using a TA-XTplus texture analyzer (Stable Micro Systems, London, UK) equipped with a tension grip system A/TG according to ASTM standard method D882.[26] Specimens of 2.5 × 8 cm rectangular strips were for tensile testing. The maximum load used in tensile measurements is 5 kg. Samples were preconditioned at 25 °C and 50 ± 3% RH in a desiccator containing magnesium nitrate saturated solution [$Mg(NO_3)_2 \cdot 6H_2O$] for at least 2 days prior to analysis. Initial gap separation and cross-head speed were set at 50 mm and 1 mm/s, respectively. TS was calculated by dividing the maximum load at break by the initial specimen cross-sectional area.[26] EAB was calculated by dividing the extension at break of the specimen by the initial guage length of the specimen (50 mm) and multiplying by 100.[26] Each trial was replicated at least eight times, and the averages were taken as the data.

Water Vapor Permeability (WVP). A modification of the ASTM E96-95 gravimetric method (1995) was employed to measure the WVP of flexible films.[27] Film samples were chosen for WVP testing on the basis of a lack of physical defects such as cracks, bubbles, or pinholes. Distilled water (15 mL) was placed in each test cup to expose the film to high relative humidity on one side through a circular opening of 4.5 cm diameter. Once the films were secured, the test cups containing films were inserted into the pre-equilibrated 0% RH desiccator cabinets and a fan was placed over the cups to ensure maintenance of moisture conditions of the film surface. Within 2 h, steady state had been achieved; the cups were weighed periodically using an analytical balance (±0.0001 g), and five weights were then

taken for each cup at >3 h intervals. The WVP (g mm kPa^{-1} m^{-2} h^{-1}) of films was calculated with the equation

$$WVP = \Delta m \times L/(A \times \Delta t \times \Delta P) \quad (3)$$

where Δm is the weight gain (g) of the glass cups during time Δt (h), L is the thickness of films (mm), A is the exposed area of films, and ΔP is the partial water vapor pressure (kPa).

DPPH Radical Scavenging Assay. The radical scavenging activity of nanoparticle-based films was measured using the stable radical DPPH according to the method of Byun et al.[28] The antioxidant capacity of the films was expressed in % DPPH radical scavenging activity/50 mg of film. Briefly, approximately 50 mg of film was placed in a flask containing 5 mL of ethyl acetate and was stirred for 1 h at room temperature (20 °C). The supernatant obtained was analyzed for DPPH radical scavenging activity. Two milliliters of methanolic solution of DPPH (40 mg/L) was mixed with 1 mL of supernatant. The control was obtained using 1 mL of ethyl acetate in the absence of the film. The mixture was vortexed vigorously and left for 30 min at room temperature in the dark. The remaining DPPH was determined by absorbance at 517 nm using a UV spectrometer. The radical scavenging activity (RSA) of the films was calculated according to the equation

$$\%\,RSA = 100 \times 1 - A_{sample}/A_{control} \quad (2)$$

where A_{sample} represents the absorbance of the sample solution and $A_{control}$ represents the absorbance of DPPH solution without the addition of the film. All experiments were carried out in triplicate.

Antimicrobial Assay. The target microorganisms selected were two Gram-negative bacteria, *E. coli* (ATCC 25922) and *Salmonella* (ATCC 14028-2). Bacterial cultures were preactivated by overnight incubation at 37 °C on Muller−Hinton (M-H) broth. The qualitative antimicrobial activity of each film was evaluated following the procedure described by Pranoto et al.[29] Films were cut into 15.0 ± 0.1 mm diameter disks using a circular knife. Film strips were then placed on M-H agar plates for bacteria that had previously been seeded with 0.1 mL of inoculum, containing 10^6 CFU/mL of each target microorganism. The plates were incubated at 37 °C for 24 h; afterward, the zones of inhibition of the film disks on the plates were examined via measuring their diameter. The test was performed in triplicate, in two separate experimental runs.

Release of Thymol from Zein−SC Nanoparticle-Based Films. Fifty milligrams of thymol-loaded nanoparticle-based films was dissolved in 5 mL of Milli-Q water, and the obtained solution was then added to a dialysis bag. The dialysis bags were incubated in 45 mL of Milli-Q water at 25 °C. An aliquot (2.5 mL) of supernatant was periodically removed while the same volume of Milli-Q water was added to keep the total volume constant at 50 mL. The absorbance of supernatant at 276 nm was recorded at 0, 1, 2, 3, 4, 6, 8, and 12 h. The cumulative amount released was integrated from each measurement, with concentrations determined from a calibration curve.

Film Thickness Determination. Film thickness was measured with a digital micrometer (TAIHAI Apparatus Co. Ltd., Shanghai, China) to the nearest 0.001 cm. Measurements were taken along the length of the specimen five times, and the mean values were used to calculate film tensile strength.

Statistics. An analysis of variance (ANOVA) of the data was performed using the SPSS 13.0 statistical analysis system, and a least significant difference (LSD) with a confidence interval of 95 or 99% was used to compare the means.

RESULTS AND DISCUSSION

Characterization of Film-Forming Nanoparticle Dispersions. The formation of zein colloidal particles through antisolvent procedures using water as antisolvent is well established,[9,30] whereas these particles did not possess water solubility, which limited to some extent their use in the food or pharmaceutical industries. When SC, an electrosteric stabilizer, was added in deionized water as an antisolvent, the zein particles were successfully coated by a layer of SC.[24] Addition of SC in the antisolvent aqueous phase did not show any major effect on the final particle size, but it caused the surface charge to shift from positive to negative and made the obtained particle retain the property of redispersibility in deionized water after freeze-drying.[24]

In preliminary experiments, we found that the zein-to-SC ratio of 1:1 was enough to stabilize zein nanoparticles and endow them with redispersibility in deionized water after freeze-drying (Figure 1A), which may heighten the stability of

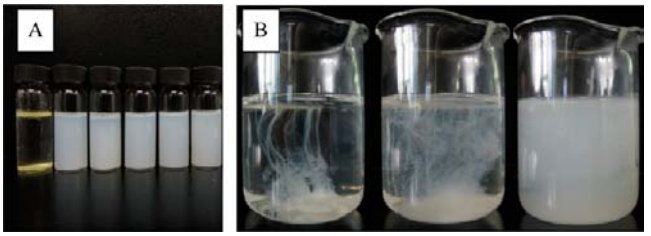

Figure 1. (A) Photograph showing the redispersion of the zein−SC nanoparticles after freeze-drying. Starting from the left, zein colloids were prepared using thymol-to-zein ratios of 0 (ZP_0), 10% (ZP_1), 20% (ZP_2), 30% (ZP_3), and 40% (ZP_4). (B) Breakdown process of the film in deionized water at various times, starting from the left, of 0, 10, and 30 s, respectively.

the formed nanoparticles during the formation of the films, and the good stability of the nanoparticles may avoid flocculation phenomena during film formation. Therefore, the films in this paper were prepared by using a zein-to-SC ratio of 1:1 to form a SC network in the outer matrix and inner zein nanoparticles, which were discretely embedded in the SC network.

Particle Size and Zeta Potential. The particle size distribution in film-forming dispersion placed a determinate role in such important characteristics of the films as microstructure, barrier, and mechanical properties. The mean particle size and surface potential of filmogenic zein−SC nanoparticle dispersions, with or without thymol, were evaluated, as summarized in Table 1. The mean particle size

Table 1. Mean Particle Size and Zeta Potential Values for Nanoparticles Prepared Using Various Zein/Thymol Ratios in the Stock Solution of 80:20 v/v Ethanol/Water

film	size (nm)	PDI	zeta potential (mV)
ZP_0	204.4 ± 12.4	0.13 ± 0.02	−38.2 ± 1.4
ZP_1	206.0 ± 3.9	0.14 ± 0.01	−44.2 ± 2.0
ZP_2	215.4 ± 21.7	0.16 ± 0.02	−44.3 ± 0.9
ZP_3	217.0 ± 8.9	0.15 ± 0.06	−45.4 ± 2.0
ZP_4	217.1 ± 14.0	0.16 ± 0.03	−44.6 ± 1.4

and zeta potential of ZP_0 were 204.4 ± 12 nm and −38.2 ± 1.4 mV, respectively. All samples have a small polydispersity index (PDI) of <0.2, indicating homogeneous size distribution of the film-forming dispersions. The particle size of ZP_0 in this study was bigger than that reported by Patel et al., who reported the particle size of zein−SC nanoparticles in the range of 120−150 nm.[24] This behavior may be attributed to the difference in zein concentrations used during the preparation of nanoparticles. In this research, the higher concentration (5%) was used to form nanoparticles before the casting process, as compared with that reported by Patel et al., who used 2.5% zein.[24] Higher

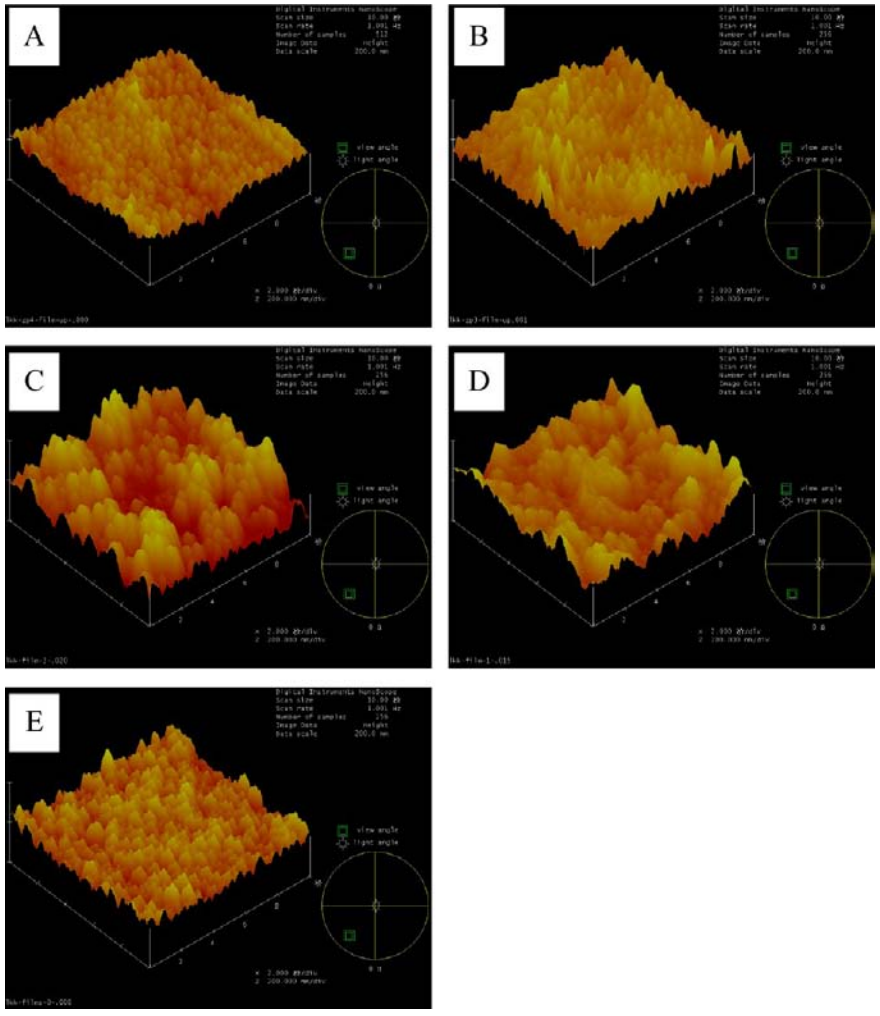

Figure 2. AFM images for zein−SC nanoparticle-based film surfaces with various thymol loadings (scaning scale, 10 μm; height scale, 100 nm): (A) ZP_0; (B) ZP_1; (C) ZP_2; (D) ZP_3; (E) ZP_4.

concentration leads to bigger particle size, which was corroborated by a previous study.[9]

As the thymol-to-zein ratios increased from 0 (ZP_0) to 40% (ZP_4), the particle size of film-forming zein−SC nanoparticle dispersions slightly increased from 204 to 217 nm, but this increase was not statistically marked (Table 1). The mean particle size of plain zein colloidal dispersion was found to be 147 ± 20 nm with a positive surface zeta potential of 34.5 mV measured at pH 4.0.[24] Addition of SC in the antisolvent aqueous phase did not show any major effect on the final particle size, but it caused the surface charge to shift from positive to negative.[24] Zeta potentials of all samples are in the range of −38 to −46 mV, indicating strong electrostatic stabilization. These observations confirmed that the SC was successfully coated on the surface of thymol-loaded zein nanoparticles. The layer of SC around zein nanoparticles may partially account for the stability of the film-forming nanoparticle-based dispersions during film formation. The obtained zein−SC nanoparticle-based films with or without thymol were light yellow, translucent, homogeneous, and smooth structures.

Solubility. Water solubility of the zein−SC nanoparticle-based films was tested to facilitate their use in food packaging. Interestingly, the obtained zein−SC nanoparticle films could automatically dissolve in warm water (40 °C), or in cold water (4 °C) after 30 s of agitation, and finally form stable colloidal dispersions (Figure 1B). There was no visible large precipitate in the colloidal dispersions, and the particle size, PDI, and zeta potential of the colloidal dispersions were 262.5 ± 7.8 nm, 0.23 ± 0.02, and −34.8 ± 0.8 mV, respectively. The particle size was slightly higher than that of the raw film-forming colloidal dispersions (262.5 vs 204.4 nm). This observation confirmed that the films were based on SC network, the zein particles in the films remaining particles within the film matrix, and consequently the ability of encapsulation and release. The ZP_4 films exhibited a similar breakdown process, with the exception of prolonged breakdown times of films matrix to about 30 min. Finally, the particle size, PDI, and zeta potential of the colloidal dispersions derived from those films were 212.2 ± 18.5 nm, 0.12 ± 0.02, and −45.5 ± 3.3 mV, respectively (data not shown).

Morphological Characterization. The effects of thymol loadings on the surface characteristics of zein−SC nanoparticle-based films were evaluated by AFM. Figure 2 shows typical surface topographies of the films, and the corresponding results of roughness parameters, the root-mean-square roughness (R_q) and average roughness (R_a), are shown in Table 2. The 3D plots were obtained for the height of the films with respect to a reference plane. Films formulated by zein−SC nanoparticles without thymol (ZP_0) showed slight surface irregularities. Clearly, the addition of thymol significantly altered the surface

Table 2. Roughness Parameters Obtained from AFM Analysis of Zein−SC Nanoparticle-Based Films with Various Thymol Loadings[a]

film	R_q[b]	R_a[c]
ZP_0	21.78 ± 3.8 c	19.04 ± 3.25 c
ZP_1	37.94 ± 6.00 b	30.71 ± 4.71 b
ZP_2	47.58 ± 2.30 a	39.03 ± 2.50 a
ZP_3	35.68 ± 3.50 b	27.87 ± 2.95 b
ZP_4	24.00 ± 4.73 c	18.78 ± 3.68 c

[a]Values are expressed as the means and standard deviation of eight measurements. Letters (a-c) indicate significant ($P < 0.05$) difference within the same column. [b]R_q, root-mean-square roughness. [c]R_a, average roughness.

morphology of the films, showing an increased trend in the surface film roughness (Figure 2). The change in the surface roughness was quantified by the R_q value, which refers to the average size of peaks and valleys within the tested area. Lower R_q numbers indicate a smoother surface. The R_q increased gradually from 21.78 to 47.58 when the thymol-to-zein ratios increased from 0 (ZP_0) to 20% (ZP_2), and decreased to 24.00 (ZP_4) upon further increasing thymol loadings (Table 2). The average roughness (R_a) presented a similar trend (Table 2). Such a trend is coherent with the aggregation behavior of zein−SC nanoparticles as the drying takes place.

Figure 3 shows the 2D AFM images of zein−SC nanoparticle-based films with or without thymol. In the ZP_0 films, the individual nanospheres with particle size about 200 nm were dominant in the film matrix. In addition, the images also show closely packed structures ontaining clusters of nanoparticles with particle size about 600 nm, probably formed by a few (two or three) raw nanoparticles (~200 nm). This result was consistent with the particle size of the film-forming nanoparticle dispersion, where the particle size and PDI of the colloidal dispersions were 204.4 ± 12.4 nm and 0.13 ± 0.02, respectively (Table 1).

Thymol loading altered the aggregation behavior of zein, with subsequent impact on microstructure of the films in a thymol loading dependent manner. In ZP_1 films, some nanoparticles were merged to form a new kind of particles with particle size about 700−800 nm, probably formed by several nanoparticles (~200 nm). The AFM images showed also closely packed structures consisting of clusters of nanoparticles with particle size ranging between 1 and 2 μm. In ZP_2 films, new particles with particle size about 700−800 nm also occurred within the film network, and several of these particles were integrated to form microscale particles, with particle size in the range of 2−3 μm (Figure 3). Furthermore, some microscale particles also accumulated together to form an enrichment region of particles with size about 3−4 μm. Those results indicated the mergence phenomenon of zein nanoparticles was distinct during the casting process when the thymol was loaded in the zein−SC nanoparticle-based films, especially ZP_2 films (Figure 3). The mergence phenomenon of zein nanoparticles resulted in bigger particles or packed structures of zein particles within the film matrix, which may affect the mechanical and/or water barrier properties of the films.

Instead, a different aggregation behavior was observed when the thymol-to-zein ratios increased to 30−40%. The individual nanospheres were visible in ZP_3 or ZP_4 films (Figure 3D,E). These nanospheres, with particle size about 300−500 nm, may

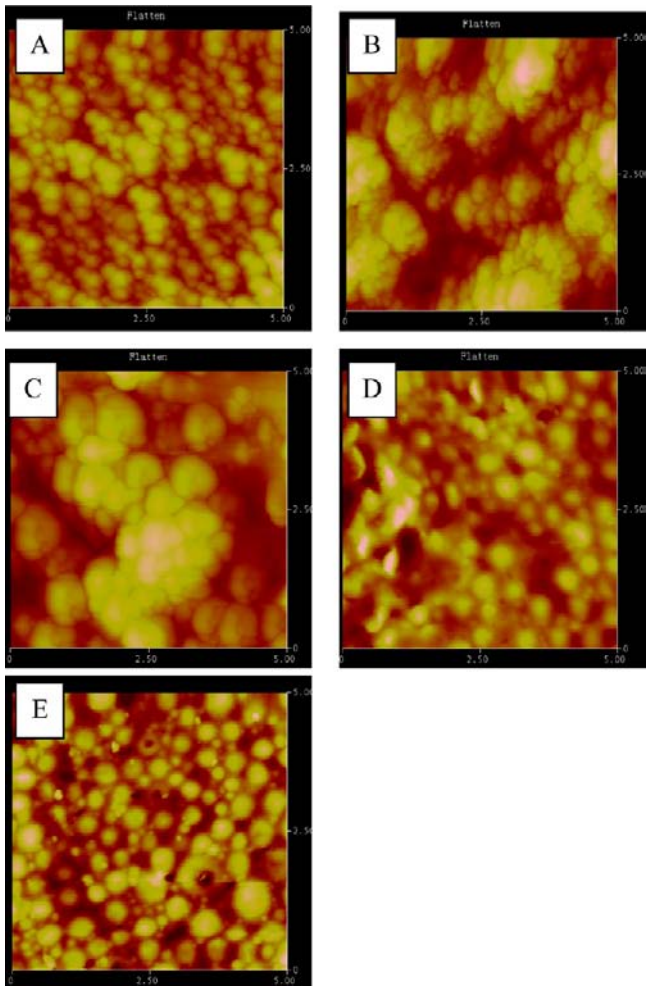

Figure 3. 2D AFM images of nanopaticle-based films with or without thymol: (A) ZP_0; (B) ZP_1; (C) ZP_2; (D) ZP_3; (E) ZP_4. Scale data: 5 × 5 μm^2.

stem from the mergence phenomena of the nanoparticles (~200 nm) as shown in film-forming dipersions or ZP_0 (control) films. Moreover, the irregular microspheres with particle size <100 nm were found in the top view of ZP_4 films (Figure 3). Most probably, the investigated thymol concentrations exceed the saturation value, causing a phase separation and yielding free thymol crystal in the SC matrix (Figure 3).

Mechanical Properties. The study of mechanical properties of edible films is a subject of great importance due to their influences on product performance. Mechanical strength and extensibility are generally required for a packaging film to maintain its integrity and withstand external stress.[31] The mechanical properties of zein−SC nanoparticle-based films with or without thymol are reported in Table 3. The TS of ZP_0 was slightly higher than that of SC film (8.88 vs 6.43 MPa), indicating the presence of nanoscale zein nanoparticles within the matrix of SC films may reinforce the internal network of the films. Zein films were usually highly brittle and showed very little elongations. The brittleness and lack of flexibility of zein films are due to the strong hydrophobic interactions that keep the zein molecules together to maintain film integrity.[32] Alkan et al. suggested the TS and EAB of zein films were about 7.2 MPa and 4%, respectively.[33] Thus, zein−SC nanoparticle-based films exhibited higher EAB values than those of the zein films,

Table 3. Tensile Properties of Zein−SC Nanoparticle-Based Films at Thymol-to-Zein Ratios of 0−40%[a]

film	TS (MPa)	EAB (%)
ZP_0	8.88 ± 0.53 a	15.67 ± 1.04 b
ZP_1	6.68 ± 0.52 b	10.70 ± 0.78 c
ZP_2	4.85 ± 0.53 c	10.97 ± 1.62 c
ZP_3	5.37 ± 0.49 c	10.83 ± 1.30 c
ZP_4	4.12 ± 0.15 d	9.94 ± 0.83 c
SC	6.43 ± 0.53 b	41.73 ± 5.6 a

[a]Values are expressed as the mean and standard deviation of eight measurements. Letters (a-d) indicate significant ($P < 0.05$) difference within the same column.

whereas their TS values were slightly higher than those of the SC films.

Although the incorporation of thymol into the zein−SC nanoparticles FFD did not significantly affect their particle size and zeta potential (Table 1), the TS of thymol-loaded nanoparticle-based films significantly ($p < 0.05$) gradually reduced from 8.88 to about 4.12 MPa as the thymol-to-zein ratios increased from 10% (ZP_1 films) to 40% (ZP_4 films). Concomitantly, the EAB decreased from 15.67 to 9.94% (Table 3). This behavior may be attributed to thymol-induced change in the self-assembly behavior of zein during the antisolvent process and film formation (Figures 2 and 3). In fact, the nanoparticles conglomerated together to form an enrichment region of nanoparticles for ZP_1 and ZP_2 films. Instead, the particles sizes in ZP_3 and ZP_4 films were about 350−500 nm, which was nearly twice as large as in ZP_0. The agglomerates or bigger particles within the film matrix may weaken the compactness of the protein network of films, with subsequent decreases in both the TS and EAB of the films.

Water Vapor Permeability (WVP). The WVP of the films is shown in Figure 4. The WVP of ZP_0 films decreased by 30%

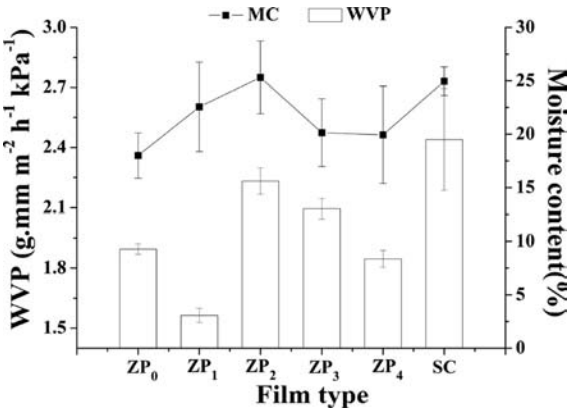

Figure 4. Water vapor permeability (WVP) and moisture content (MC) of zein−SC nanoparticle-based films with or without thymol.

when compared with that of SC films. The ZP_0 films possessed improved water vapor barrier, which may be related to the fact that the zein nanoparticles, which are hydrophobic particles, remained homogeneously distributed in the protein network of the dry film matrix because it increased the tortuosity factor of the vapor diffusion path through films. Unexpectedly, the loading of thymol, a hydrophobic antimicrobial, weakened the water barrier capability of the films, in a thymol loading dependent manner (Figure 4). Interestingly, the WVP of the films increased from 1.68 g mm kPa^{-1} m^{-2} h^{-1} (ZP_0) to 2.23 g mm kPa^{-1} m^{-2} h^{-1} (ZP_2) when the thymol-to-zein ratios were increased to 20% and then decreased to 1.85 g mm kPa^{-1} m^{-2} h^{-1} (ZP_4 films) upon further increase in the thymol loadings.

This unexpected response of the WVP to thymol loading was consistent with the microstructure of the films, further confirming that the reduced continuity and cohesion of the protein network due to the presence of large agglomerates of nanoparticles in the films matrix might facilitate the migration of water vapor. The appearance of free thymol crystal-like particles in the film matrix, with size lower 100 nm in AFM images (Figure 3E), may account for the improved water barrier capability as the thymol-to-zein ratios increased gradually from 20 to 40%. Therefore, it cannot be assumed that the WVP of edible films is reduced simply by adding a hydrophobic component to the formulation.

Moisture Content (MC). Packaging films should maintain moisture levels within the packaged product. Therefore, knowledge of the MC of the film is very important for food packaging applications. The MC of zein−SC nanoparticle-based films with or without thymol is shown in Figure 4. ZP_0 films possessed lower MC than SC films, which may be related to the fact that the zein nanoparticles, hydrophobic particles, remained homogeneously distributed in the dry film matrix. Unexpectedly, the loading of thymol, a hydrophobic antimicrobial, increased the MC of zein−SC nanoparticle-based films in a thymol-loading dependent manner (Figure 4). The MC of the films increased from 18.0 ± 2.0% (ZP_0) to 25.3 ± 3.4% (ZP_2) when the thymol-to-zein ratios were increased to 20% and then decreased to about 19.9 ± 4.6% (ZP_4 films) upon further increase in the thymol loadings. Interestingly, the WVP and MC exhibited a similar trend with increasing thymol loadings. This unexpected response of the MC to thymol loading was consistent with the microstructure of the films, further indicating that the reduced continuity and cohesion of the protein network due to the presence of large agglomerates of nanoparticles in the films matrix might facilitate the enrichment of the plasticizer (glycerol, an effective plasticizer) in gaps among the aggregate-based clusters, with subsequent increase in water adhesion capacity.

DPPH Radical Scavenging Activity. The DPPH radical has been widely used to test the ability of compounds as free radical scavengers or hydrogen donors to evaluate antioxidant activity. DPPH tests were conducted to evaluate whether thymol, a natural antioxidant agent, retained its antioxidant capacity during incorporation in zein−SC nanoparticle films. Figure 5 presents the radical scavenging activity as a function of thymol-to-zein ratios, which was found to be concentration dependent. ZP_0 films showed radical scavenging activity of 10% on DPPH, which may be mainly attributed to the capacity of remain small molecule such as peptide and phenols in zein. As the thymol-to-zein ratios increased from 0 to 40%, the DPPH scavenging activity increased from 25 to 52%, indicating the addition of thymol within the film matrix retained its antioxidant ability.

Antimicrobial Properties. The antimicrobial activity of films was evaluated using the agar diffusion method. The indicator bacteria used for examination, *E. coli* and *Salmonella*, are common food human pathogens (meat). The inhibitory activity was measured on the basis of the clear zone surrounding the circular filmstrips. The typical halo images of the films against *E. coli* are shown in Figure 6, and the related inhibition zone diameters of the films are shown in Table 4. The inhibitory activity of the films against the test bacteria

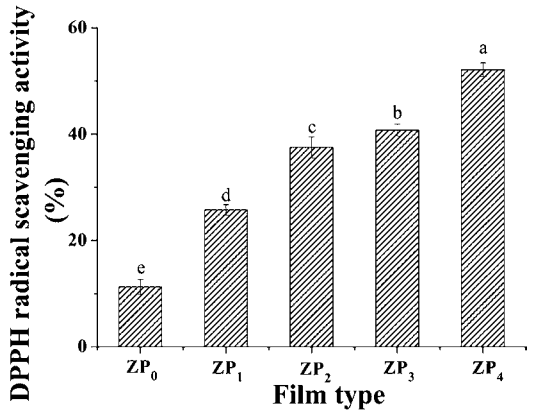

Figure 5. DPPH radical scavenging activity of thymol-loaded zein−SC nanoparticle-based films.

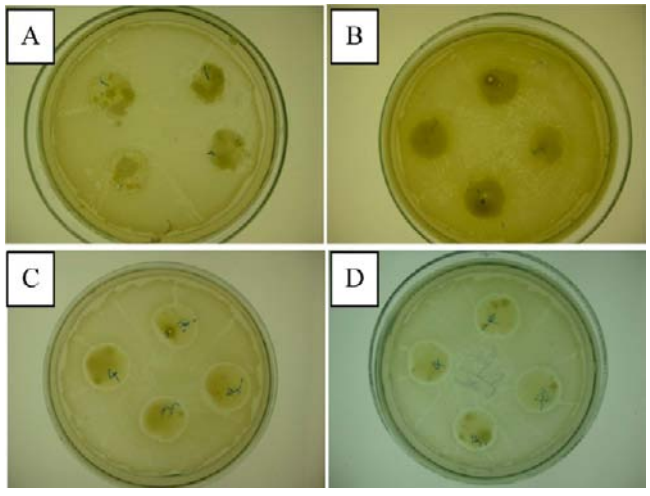

Figure 6. Antibacterial activity of zein−SC nanoparticle-based films against *E. coli* on agar surface diffusion assay.

Table 4. Zones of Inhibition for Zein−SC Nanoparticle-Based Films with or without Thymol[a]

	zone of inhibition (mm)	
film	*E. coli*	*Salmonella*
ZP_0	–[b]	–
ZP_1	–	–
ZP_2	15.89 ± 0.74 b	16.02 ± 0.28 b
ZP_3	16.95 ± 0.59 ab	17.23 ± 0.98 ab
ZP_4	18.81 ± 0.56 a	18.12 ± 1.04 a

[a]Values represent the mean and standard deviation of inhibition zones from three experiments. Letters (a-b) indicate significant ($P < 0.05$) difference within the same column. [b]No zones of inhibition.

depended on the loading of thymol. No significant inhibition halos were induced by the ZP_0 and ZP_1 films for any of the pathogens analyzed (Figure 6 and Table 4). In fact, there were a lot of colonies on the surface of the ZP_0 films, whereas there were a lot of colonies of the indicator bacteria on the plate but not on the surface of the ZP_1 films (Figure 6A,B). Moreover, the test bacteria (*E. coli* and *Salmonella*) were sensitive to the zein−SC nanoparticle-based films at thymol-to-zein ratios of 30−40%, evidenced by visible halo zones around those filmstrips, and the diameter of the inhibition zone increased from about 16 to 18 mm in a thymol loading dependent manner (Figure 6 and Table 4).

Release Properties. Figure 7 presents the in vitro release profiles of thymol from zein−SC nanoparticle-based films, as a

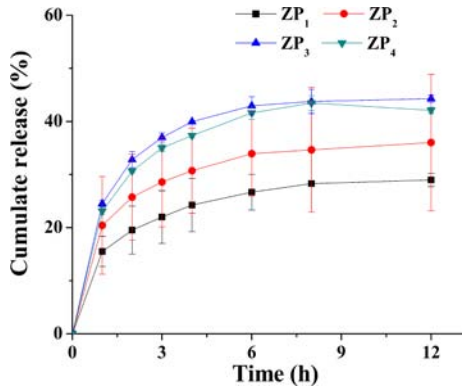

Figure 7. Release of thymol-loaded zein−SC nanoparticle-based films.

function of thymol-to-zein ratios. The release kinetic profile of thymol from zein−SC nanoparticle-based films can be described as a two-step biphasic process, that is, an initial burst effect followed by a subsequent slower release. Thymol release from the nanoparticle-based films was dependent on thymol loadings. At low thymol-to-zein ratios (e.g., 10 or 20%), the burst effect occurred within 1.5 h and about 28% encapsulated thymol released from the films. As the thymol-to-zein ratios increased, the burst effect was dramatically strengthened and the accumulative release after 6.5 h was increased from 28 to 44% (ZP_3 or ZP_4 films) (Figure 7).

In fact, the film networks were rapidly destroyed as the films were thrown in deionized water (Figure 1B). The zein−SC nanoparticle films could automatically dissolve in warm water (40 °C), or in cold water (4 °C) after 30 s of agitation, and finally form stable colloidal dispersions. However, the accumulative releases after 6.5 h from the films were about 28−44% (ZP_1−ZP_4 films). These phenomena indicated that most of the thymol in the films was loaded on zein nanoparticles, which were embedded in the SC network. Instead, zein−SC nanoparticles endowed the films with the ability to sustain release of thymol. Thus, the free thymol within the film matrix may partially account for the burst releases of thymol. Furthermore, thymol was preferably retained within the nanoparticles, which was supported by the fact that thymol, a phenolic compound, is capable of forming H-bonding with zein, a proline-rich protein. Polyphenolic compounds are known to interact with prolamin residues of proteins via hydrophobic interaction and hydrogen bonding.[34,35]

Schematic Illustration. The zein−SC nanoparticle films could automatically dissolve in warm water (40 °C), or in cold water (4 °C), and finally form stable colloidal dispersions. The cumulative release of thymol after 6.5 h was in the range of 28−44% at various thymol loadings, indicating that zein−SC nanoparticles endowed the films with the ability to sustain release of thymol. However, the encapsulation efficiency of directly freeze-dried ZP_1 nanoparticle dispersions was only about 36%, where the solutions were frozen and free thymol was immovable during the freeze-drying. During the formation process of films, thymol molecules may tend to migrate to the uncovered surface or core of zein nanoparticles by hydrophobic interactions, in view of the fact that ethanol evaporation was

rapid than in water, resulting in an increase in solvent polarity in the FFD. These phenomena suggested the possible migration mechanism of thymol to the core or surface of zein nanoparticles during solvent evaporation and film network formation.

Herein, a schematic illustration of the formation of zein−SC nanoparticle-based films with or without thymol is proposed and shown in Figure 8. In the case of ZP_0, zein particles may

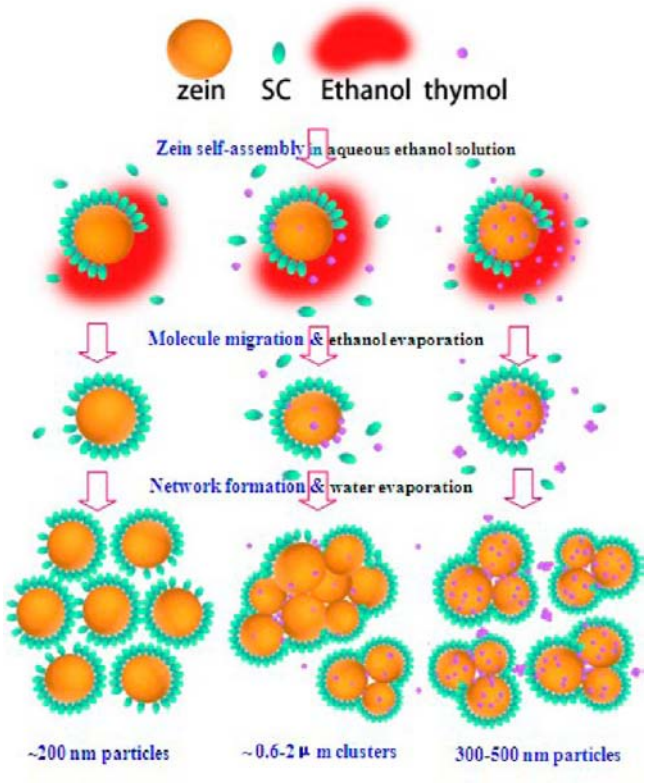

Figure 8. Schematic illustration of formation of zein−SC nanoparticle-based films with or without thymol: (left) films without thymol (ZP_0); (middle) films at thymol-to-zein ratios of 10 and 20% (ZP_1 or ZP_2); (right) films at thymol-to-zein ratios of 30 and 40% (ZP_3 or ZP_4).

not be perfectly covered by SC after antisolvent procedure due to about 22% residual ethanol in the FFD. Thus, ethanol may surround the uncovered surface of zein and prevent free SC from absorbing to it. During the film-drying process, ethanol content declined and free SC was absorbed onto the particle surface. Ethanol evaporation was accompanied by SC migration toward the exposed surface or the core of zein particles. The coating layer of SC around zein nanoparticles endowed the casting films with dispersibility in deionized water (Figure 8, left).

In ZP_1 or ZP_2 films in which the thymol-to-zein ratios were 10 or 20%, thymol loading in film formulation was moderate, and the thymol molecule may mainly surround the uncovered surface of zein where most of the residual ethanol occurred. It may migrate to the core or uncovered particle surface due to solvent evaporation, and the deposit of thymol on the surface of the particles can block the absorption of SC. Therefore, those particles may aggregate to form bigger particles (~600−800 nm) or an agglomerate of particles (Figure 8, middle). Thus, the presence of agglomerates of particles may weaken the compactness of the protein network of films, forming some gaps among agglomerates or particles, where the glycerol or water may be rich, and thus impaired the water barrier capacity, mechanical resistance, and extensibility (Table 3 and Figure 4).

In ZP_3 or ZP_4 films, the thymol-to-zein ratios were 30 or 40%, respectively. The thymol amount in the formulation may be superabundant. During solvent evaporation, thymol concentrations in some regions may exceed its saturation value, causing a phase separation and yielding free thymol crystals in the film matrix before their migration to the uncovered particle surface. This behavior was supported by AFM experiments, where free thymol crystal-like particles with particle size lower than 100 nm were observed (Figure 2E). Instead, the thymol molecule being adjacent zein nanoparticles may be able to migrate toward the uncovered surface of zein nanoparticles before the formed thymol supersaturated droplet during the film-drying process. The moderate coverage of thymol on zein nanoparticles may result in slight mergence phenomenon, with subsequent formation of nanoparticles, with particle size about 350−500 nm. These particles remained homogeneously distributed in the protein network of the dry film matrix, and the presence of free thymol crystal in the film matrix may account for the improved water barrier capacity when compared with those of ZP_2 films (Figure 3), because those particles and free thymol crystals increased the tortuosity factor of the vapor diffusion path through films.

In conclusion, thymol-loaded zein−SC nanoparticles were prepared using antisolvent techniques. Thymol loadings endowed zein-SC nanoparticle-based films with antimicrobial activity against *E. coli* and *Salmonella* as well as DPPH radical scavenging activity. The release kinetic profile of thymol from zein/SC nanoparticles-based films can be described as a two-step biphasic process, that is, an initial burst effect followed by subsequent slower release. The migration of thymol during film formation altered the zein self-assembly, to form various particles or packed structure. This difference in microstructure partially accounted for the impaired mechanical and barrier properties of thymol-loaded nanoparticle-based films. The present data indicated that the thymol-loaded films, for example, ZP_3 or ZP_4 films, could be used as an inner packaging for foods such as the flavoring of instant noodles in view of their antimicrobial and antioxidant activities, as well as water solubility.

AUTHOR INFORMATION

Corresponding Author

*(S.-W.Y.) Phone: +86-20-87114262. Fax: +86-20-87114263. E-mail: feysw@scut.edu.cn. (X.-Q.Y.) Phone: +86-20-87114262. Fax: +86-20-87114263. E-mail: fexqyang@scut.edu.cn.

Funding

We acknowledge financial support from the Natural Science Fund of Guangdong Province, China (10451064101005149), the Fundamental Research Funds for the Central Universities (SCUT, 2012ZZ0082), the Open Project Program of State Key Laboratory of Pulp and Paper Engineering, South China University of Technology (No. 201023), the Open Project Program of Guangdong Province Key Laboratory for Green Processing of Natural Products and Product Safety (201102), and the project supported by the State Key Program of National Natural Science of China (No. 31130042).

Notes

The authors declare no competing financial interest.

REFERENCES

(1) De Roever, C. Microbiological safety evaluations and recommendations on fresh produce. *Food Control* **1998**, *9*, 321−347.

(2) López, P.; Sánchez, C.; Batlle, R.; Nerín, C. Development of flexible antimicrobial films using essential oils as active agents. *J. Agric. Food Chem.* **2007**, *55*, 8814−8824.

(3) Restuccia, D.; Spizzirri, U. G.; Parisi, O. I.; Cirillo, G.; Curcio, M.; Lemma, F.; Puoci, F.; Vinci, G.; Picc, N. New EU regulation aspects and global market of active and intelligent packaging for food industry applications. *Food Control* **2010**, *21*, 1425−1435.

(4) Suppakul, P.; Miltz, J.; Sonneveld, K.; Bigger, S. W. Active packaging technologies with an emphasis on antimicrobial packaging and its applications. *J. Food Sci.* **2003**, *68*, 408−420.

(5) Mariniello, L.; Di Pierro, P.; Esposito, C.; Sorrentino, A.; Masi, P.; Porta, R. Preparation and mechanical properties of edible pectin-soy flour films obtained in the absence or presence of trans-glutaminase. *J. Biotechnol.* **2003**, *102*, 191−198.

(6) Ou, S. Y.; Kwok, K. C.; Kang, Y. J. Changes in *in vitro* digestibility and available lysine of soy protein isolate after formation of film. *J. Food Eng.* **2004**, *64*, 301−305.

(7) Liu, X.; Sun, Q.; Wang, H.; Zhang, L. K.; Wang, J. Y. Microspheres of corn protein, zein, for an ivermectin drug delivery system. *Biomaterials* **2005**, *26*, 109−115.

(8) Hurtado-López, P.; Murdan, S. Zein microspheres as drug/antigen carriers: a study of their degradation and erosion, in the presence and absence of enzymes. *J. Microencapsul.* **2006**, *23*, 303−314.

(9) Zhong, Q. X.; Jin, M. F. Nanoscalar structures of spray-dried zein microcapsules and *in Vitro* release kinetics of the encapsulated lysozyme as affected by formulations. *J. Agric. Food Chem.* **2009**, *57*, 3886−3894.

(10) Wu, L. Y.; Wen, Q. B.; Yang, X. Q.; Xu, M. S.; Yin, S. W. Wettability, surface microstructure and mechanical properties of films based on phosphorus oxychloride-treated zein. *J. Sci. Food Agric.* **2011**, *91*, 1222−1229.

(11) O'Donnell, P. B.; Wu, C. B.; Wang, J. J.; Wang, L.; Oshlack, B.; Chasin, M.; Bodmeier, R.; McGinity, J. W. Aqueous pseudolatex of zein for film coating of solid dosage forms. *Eur. J. Pharm. Biopharm.* **1997**, *43*, 83−89.

(12) Persico, P.; Ambrogi, V.; Carfagna, C.; Cerruti, P.; Ferrocino, I.; Mauriello, G. Nanocomposite polymer films containing carvacrol for antimicrobial active packaging. *Polym. Eng. Sci.* **2009**, *49*, 1447−1455.

(13) Valentao, P.; Fernandes, E.; Carvalho, F.; Andrade, P. B.; Seabra, R. M.; Bastos, M. L. Antioxidative properties of cardoon (*Cynara cardunculus* L.) infusion against superoxide radical, hydroxyl radical, and hypochlorous acid. *J. Agric. Food Chem.* **2002**, *50*, 4989−4993.

(14) Marino, M.; Bersani, C.; Comi, G. Antimicrobial activity of the essential oils of *Thymus vulgaris* L. measured using a bio-impedometric method. *J. Food Prot.* **1999**, *62*, 1017−1023.

(15) Altieri, C.; Speranza, B.; Del Nobile, M. A.; Sinigaglia, M. Suitability of bifidobacteria and thymol as biopreservatives in extending the shelf life of fresh packed plaice fillets. *J. Appl. Microbiol.* **2005**, *99*, 1294−1302.

(16) Valero, D.; Valverde, J. M.; Martinez-Romero, D.; Guillen, F.; Castillo, S.; Serrano, M. The combination of modified atmosphere packaging with eugenol or thymol to maintain quality, safety and functional properties of table grapes. *Postharvest Biol. Technol.* **2006**, *41*, 317−327.

(17) Falcone, P. M.; Speranza, B.; Del Nobile, M. A.; Corbo, M. R.; Sinigaglia, M. A study on the antimicrobial activity of thymol intended as a natural preservative. *J. Food Prot.* **2005**, *68*, 1664−1670.

(18) Zhou, F.; Ji, B.; Zhang, H.; Jiang, H.; Yang, Z.; Li, J.; Li, J.; Yan, W. The antibacterial effect of cinnamaldehyde, thymol, carvacrol and their combinations against the foodborne pathogen *Salmonella* typhimurium. *J. Food Saf.* **2007**, *27*, 124−133.

(19) Sikkema, J.; J. de Bont, A. M.; Poolman, B. Interactions of cyclic hydrocarbons with biological membranes. *J. Biol. Chem.* **1994**, *269*, 8022−8028.

(20) Buonocore, G. G.; Del Nobile, M. A.; Panizza, A.; Bove, S.; Battaglia, G.; Nicolais, L. Modeling the lysozyme release kinetics from antimicrobial films intended for food packaging applications. *J. Food Sci.* **2003**, *68*, 1365−1370.

(21) Del Nobile, M. A.; Conte, A.; Incoronato, A. L.; Panza, O. Antimicrobial efficacy and release kinetics of thymol from zein films. *J. Food Eng.* **2008**, *89*, 57−63.

(22) Mastromatteo, M.; Barbuzzi, G.; Conte, A.; Del Nobile, M. A. Controlled release of thymol from zein based film. *Innovative Food Sci. Emerging Technol.* **2009**, *10*, 222−227.

(23) Dickinson, E. Properties of emulsions stabilized with milk proteins: overview of some recent developments. *J. Dairy Sci.* **1997**, *80*, 2607−2619.

(24) Patel, A.; Bouwens, E. C. M.; Velikov, K. P. Sodium caseinate stabilized zein colloidal particles. *J. Agric. Food Chem.* **2010**, *58*, 12497−12503.

(25) Patel, A.; Hu, Y. C.; Tiwari, J. K.; Velikov, K. P. Synthesis and characterisation of zein−curcumin colloidal particles. *Soft Matter* **2010**, *6*, 6192−6199.

(26) ASTM. Standard test method for tensile properties of thin plastic sheeting. Standard Designation: D882. In *Annual Book of ASTM Standards*; American Society for Testing Materials: Philadelphia, PA, 2001.

(27) McHugh, T. H.; Avena-Bustillos, R.; Krochta, J. M. Hydrophilic edible films: modified procedure for water vapor permeability and explanation of thickness effects. *J. Food Sci.* **1993**, *58*, 899−903.

(28) Byun, Y.; Kim, Y. T.; Whiteside, S. Characterization of an antioxidant polylactic acid (PLA) film prepared with a-tocopherol, BHT and polyethylene glycol using film cast extruder. *J. Food Eng.* **2010**, *100*, 239−244.

(29) Pranoto, Y.; Salokhe, V. M; Rakshit, S. K. Physical and antibacterial properties of alginate-based edible film incorporated with garlic oil. *Food Res. Int.* **2005**, *38*, 267−272.

(30) Parris, N.; Cooke, P. H.; Hicks, K. B. Encapsulation of essential oils in zein nanospherical particles. *J. Agric. Food Chem.* **2005**, *53*, 4788−4792.

(31) Yang, L.; Paulson, A. T. Effects of lipids on mechanical and moisture barrier properties of edible gellan film. *Food Res. Int.* **2000**, *33*, 571−578.

(32) Guo, Y.; Liu, Z.; An, H.; Li, M.; Hu, J. Nano-structure and properties of maize zein studied by atomic force microscopy. *J. Cereal Sci.* **2005**, *41*, 277−281.

(33) Alkan, D.; Aydemir, L. Y.; Arcan, I.; Yavuzdurmaz, H.; Atabay, H. I.; Ceylan, C.; Yemenicioğlu, A. Development of flexible antimicrobial packaging materials against *Campylobacter jejuni* by incorporation of gallic acid into zein-based films. *J. Agric. Food Chem.* **2011**, *59*, 11003−11010.

(34) Emmambux, N. M.; Taylor, J. R. N. Sorghum kafirin interaction with various phenolic compounds. *J. Sci Food Agric.* **2003**, *83*, 402−407.

(35) Taylor, J.; Taylor, J. R. N.; Belton, P. S.; Minnaar, A. Kafirin microparticle encapsulation of catechin and sorghum condensed tannins. *J. Agric. Food Chem.* **2009**, *57*, 7523−7528.